Applied Clay Science 42 (2008) 39–49

Contents lists available at ScienceDirect

Applied Clay Science

journal homepage: www.elsevier.com/locate/clay

Poly (styrene) latex/modified Na-activated bentonite nanocomposite films: A fluorescence study

Şaziye Uğur [a,*], Önder Yargı [a], Ebru Günister [a], Önder Pekcan [b]

[a] Istanbul Technical University, Department of Physics, 34469 Maslak, Istanbul, Turkey
[b] Işık University, Department of Physics, Şile,34980 Istanbul, Turkey

ARTICLE INFO

Article history:
Received 6 June 2007
Received in revised form 25 January 2008
Accepted 13 February 2008
Available online 4 March 2008

Keywords:
Composite
Void closure
Interdiffusion
Fluorescence
Polystyrene latex
Bentonite

ABSTRACT

We studied film formation of composites of surfactant-free polystyrene (PS) nanoparticles and modified Na-activated bentonite (MLB), by steady state fluorescence (SSF) technique. The films were prepared from a mixture of pyrene (P)-labeled PS particles and MLB at various compositions at room temperature. These films were annealed at elevated temperatures above the glass transition (T_g) temperature of polystyrene for 10 min. Scattered light (I_s) and fluorescence intensities (I_P) from P were measured after each annealing step to monitor the stages of film formation. Evolution of transparency of the composite films was monitored by using photon transmission intensity, I_{tr}. Atomic force microscopy (AFM) was used to detect the variation in physical structure of annealed composite films. The nanocomposite films exhibited a percolation threshold at 20 wt.% MLB content. Below this fraction two distinct film formation stages were observed which are known as void closure and interdiffusion and above this fraction no film formation was detected. At 0–20 wt.% MLB, minimum film formation, T_0, void closure, T_v and healing, T_h temperatures were determined. Void closure and interdiffusion stages were modeled and related activation energies were determined. Void closure activation energies decreased as the percent of MLB increased, no variation was observed in backbone activation energies.

© 2008 Elsevier B.V. All rights reserved.

1. Introduction

Film formation from soft (low-T_g) and hard (high-T_g) latex dispersions can occur in several stages. In both cases, the first stage corresponds to the wet initial stage. Evaporation of solvent leads to second stage in which the particles form a close packed array, here if the particles are soft they are deformed to polyhedrons. Hard latex particles remain essentially discrete and undeformed during drying. The mechanical properties of such films can be evolved after all the solvent is evaporated by annealing process. Annealing of soft particles causes diffusion across particle–particle boundaries which lead to a homogeneous continuous material. In the annealing of hard latex system, however, deformation of particles first leads to void closure (Mackenzie and Shuttleworth, 1949; Sperry et al., 1994; Mazur, 1995) and then after the voids disappeared diffusion across particle–particle boundaries starts. The last stage of film formation is the coalescence of the particles where macromolecules belonging to different particles mix by interdiffusion (Pekcan and Arda, 1999).

In the last decade, there has been growing interest in producing new materials by filling polymers with inorganic natural and/or synthetic compounds. Since the inorganic particles display rather macroscopic dimensions and since there is mostly no interaction between the two mixed components at the interface between the two partners, the resulting composite materials can be seen as filled polymers. In recent years, Polymer/clay (P/C) nanocomposites have become increasingly important because they combine the structural, physical and chemical properties of both clay minerals and polymer. The clay mineral modifies many different properties of the polymer, such as absorbancy, ion exchange capability, and thermal and solvent resistance. They give improved mechanical properties, gas barrier properties and decreased flammability (Li et al., 2003). The improved composites are widely used in areas such as construction, electronic, consumer products, and transportation (Salahuddin and Akelah, 2002).

The synthesis of nylon/clay nanocomposites via in-situ polymerization produced polymer/clay minerals (Giannelis, 1996; Le Baron et al., 1999; Alexandre and Dubais, 2000; Collister, 2002) where the addition of only a few percent of clay minerals changed the properties of the material significantly. Several procedures are known in the incorporation of clay minerals into a polymer matrix in the dispersed manner (Usuki et al., 1993). Intercalated composites formed by the incorporation of only one or two polymeric chains between the layers of the minerals have been reported (Aranda and Ruizhitzky, 1992; Wu and Lerner, 1993). Composites with polyetheneoxide have been studied by simple mixing of the molten polymer with layered minerals (Vaia et al., 1995). The incorporation of montmorillonite into polypropylene was reported where the compatibilizing ability of

* Corresponding author. Tel.: +90 212 2856603; fax: +90 212 2856386.
E-mail address: saziye@itu.edu.tr (Ş. Uğur).

0169-1317/$ – see front matter © 2008 Elsevier B.V. All rights reserved.
doi:10.1016/j.clay.2008.02.009

the functionalized oligomers was studied (Kawasumi et al., 1997). Recently clay minerals were investigated as compatibilizer for immiscible poly(propylene)/polystyrene blends (Wang et al., 2003).

Polystyrene (PS) is one of the most popular and widely-used polymers. Several attempts to prepare polystyrene–clay mineral composites have been reported (Friedlander and Grink, 1964; Kato et al., 1981; Vara et al., 1996; Doh and Cho, 1998; Noh and Lee, 1999; Ugur et al., 2005, 2006). Many researchers are interested in studies of PS–clay nanocomposites (Vara et al., 1996; Noh and Lee, 1999). A common technique involves impregnating of clay in styrene monomer followed by polymerization. Recently, Doh and Cho (1998) prepared polystyrene–clay intercalated nanocomposites by polymerization of styrene in the presence of organophilic clay. The intercalated polystyrene–clay nanocomposites exhibited thermal stability better than pure polystyrene. Giannelis et al. reported that the intercalation of PS into organophilic clay mineral interlayer spaces can be achieved by heating a mixture of PS and organophilic clay mineral above the glass transition temperature of PS (Vara et al., 1996). Lee et al. demonstrated the synthesis and characterization of PS–clay nanocomposites by emulsion polymerization (Noh and Lee, 1999). Recently, we have prepared the polystyrene/Na-activated bentonite nanocomposites (Ugur et al., 2005, 2006) by blending and analysed the film formation behavior by SSF and UVV techniques. The addition of a small amount of clay (7 wt.%) prevented film formation process.

In this study, the evolution of film formation from composites of modified Na-activated bentonite (MLB) and nanosized polystyrene (PS) latex was studied. Steady state fluorescence (SSF) and photon transmission (UVV) techniques were used to monitor the film formation stages depending on annealing temperature ranging from 100 to 280 °C. Film formation stages were modeled and related activation energies were determined.

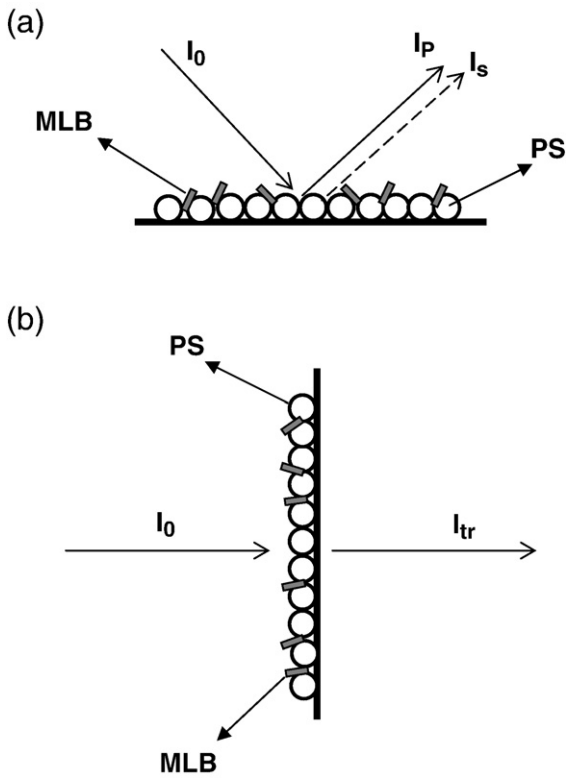


Fig. 2. Schematic illustration of sample position and a — incident light (I_0), scattered light (I_s) and P emission (I_P) intensities, b — transmitted light intensity (I_{tr}).

2. Experimental

2.1. Materials

2.1.1. Modified Na-activated bentonite (MLB)

The Na-activated bentonite (NaLB) was obtained from bentonite collected from the bentonite deposits in Lalapaşa-Edirne, Thrace, Turkey (courtesy of Bensan Corp.) by treating with 4% (w/w) $NaHCO_3$ solution. NaLB was dispersed in distilled water at room temperature for 24 h (6 wt.% NaLB stock dispersion). The pH value of NaLB was 10.7. Benzyldimethyl tetradecylammonium chloride (BDTDACl) was dissolved in water at 20 mmol/l concentration. The mixture of 5 ml BDTDACl stock solution, 6.25 ml 6 wt.% NaLB stock dispersion and 1.25 ml water was shaken to get 3 wt.% NaLB and 8 mmol/l BDTDACl (modified Na-activated bentonite). This dispersion was shaken overnight for 24 h. The dispersion was diluted to obtain 0.0141 g/ml MLB.

The particle size distribution (PSD) of the bentonite was determined by the sedimentation technique. A photocentrifugal Particle Size Analyser SA-CP2 model Shimadzu Corp., was used. The PSD of the NaLB was in the range of 50–0.4 μm and the average particle size was 10 μm (Fig. 1). After the modification, the PSD of MLB was 10–0.4 μm and the average particle size was 1 μm. In original NaLB dispersion, the fraction of particles larger than 10 μm was 49.8%, no particles above 10 μm were found after addition of BDTDACl (Günister et al., 2006, 2007). While particle size was decreasing, the surface area of these particles increased. BDTDACl can help to break the huge clay mineral flocs.

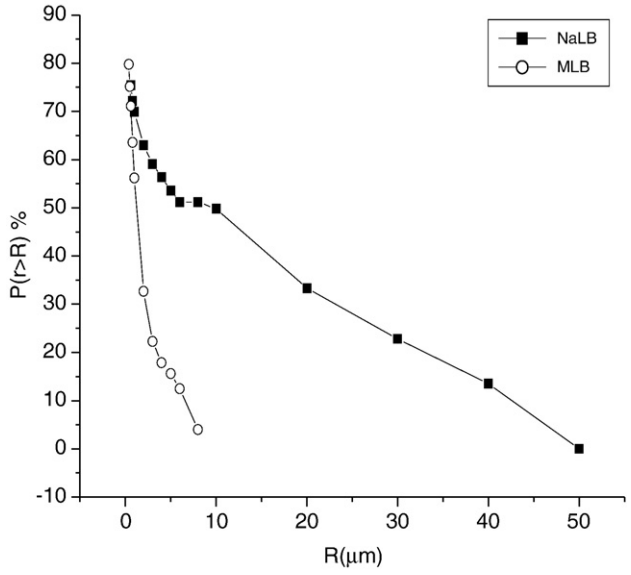


Fig. 1. Particle size distributions for natural NaLB and MLB.

2.1.2. PS latex

Pyrene-labeled polystyrene particles were synthesized via emulsifier-free polymerization. The polymerization reaction was carried out in a 200 ml thermostated

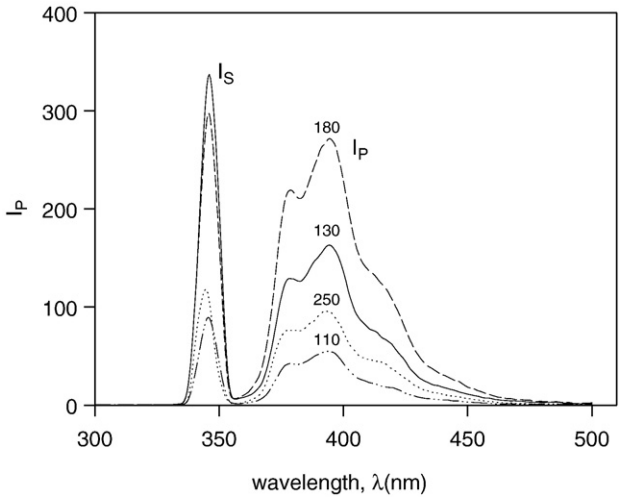


Fig. 3. Emission (I_P) and scattered (I_s) spectra of latex films after being annealed at various temperatures for 10 min. Numbers show annealing temperatures in °C.

round-bottomed four-necked flask, equipped with a glass anchor-shaped stirrer, condenser and nitrogen inlet. Styrene monomer was first introduced in the reactor containing boiled and deionised water and then the fluorescent monomer 1-pyrenylmethyl methacrylate (PolyFluor™394) was dissolved in a small amount of styrene. The potassium persulfate (KPS) initiator was dissolved in water and added when the polymerization temperature was constant at 70 °C. The stirring rate was adjusted to 300 rpm. The recipe: 100 ml water, 4 g of styrene, 0.1 g of KPS (dissolved in 2 ml water) and 0.0129 g of fluorescent monomer (dissolved in 1 g styrene). The polymerization reaction was performed during 18 h under nitrogen atmosphere. The particles are spherical and fairly monodisperse, and have a mean diameter of 320 nm.

2.2. Film preparation

PS/MLB composite films were prepared by casting. Distilled water was used to disperse the used materials. 0, 3, 5, 7, 10, 20, 30 and 50 wt.% MLB content films were prepared. Dried films were obtained by placing the same number of drops from these dispersions on a glass plates with the size of 0.8×2.5 cm^2 and allowing the water to evaporate. The film samples were separately annealed above T_g of PS, 105 °C, for 10 min at temperatures 100 to 280 °C. The temperature was maintained within ±2 °C during annealing.

After annealing, each sample was placed in the solid surface accessory of a Perkin Elmer Model LS-50 fluorescence spectrometer. Pyrene (P) was excited at 345 nm and scattered light and fluorescence emission were detected between 300 and 500 nm. All measurements were carried out in the front-face position at room temperature. Slit widths were kept to provide the resolution of 8 nm during all SSF measurements. The sample position, incident, I_0, scattered, I_s light and P emission intensity, I_P are shown in Fig. 2a, I_s is collected at right angle with respect to incident light. Photon transmission measurements were performed by using Lambda 35 UV–Visible spectrometer from Perkin Elmer. The transmittance of the films was measured at 400 nm. A glass plate was used as a standard for all UVV experiments, the measurements were carried out at room temperature after each annealing processes. The sample position and schematic sketch of the light passed (I_{tr}) are presented in Fig. 2b. Atomic Force Microscopy (AFM) images were obtained by SPM-9500-J3 Shimadzu scanning probe microscopy.

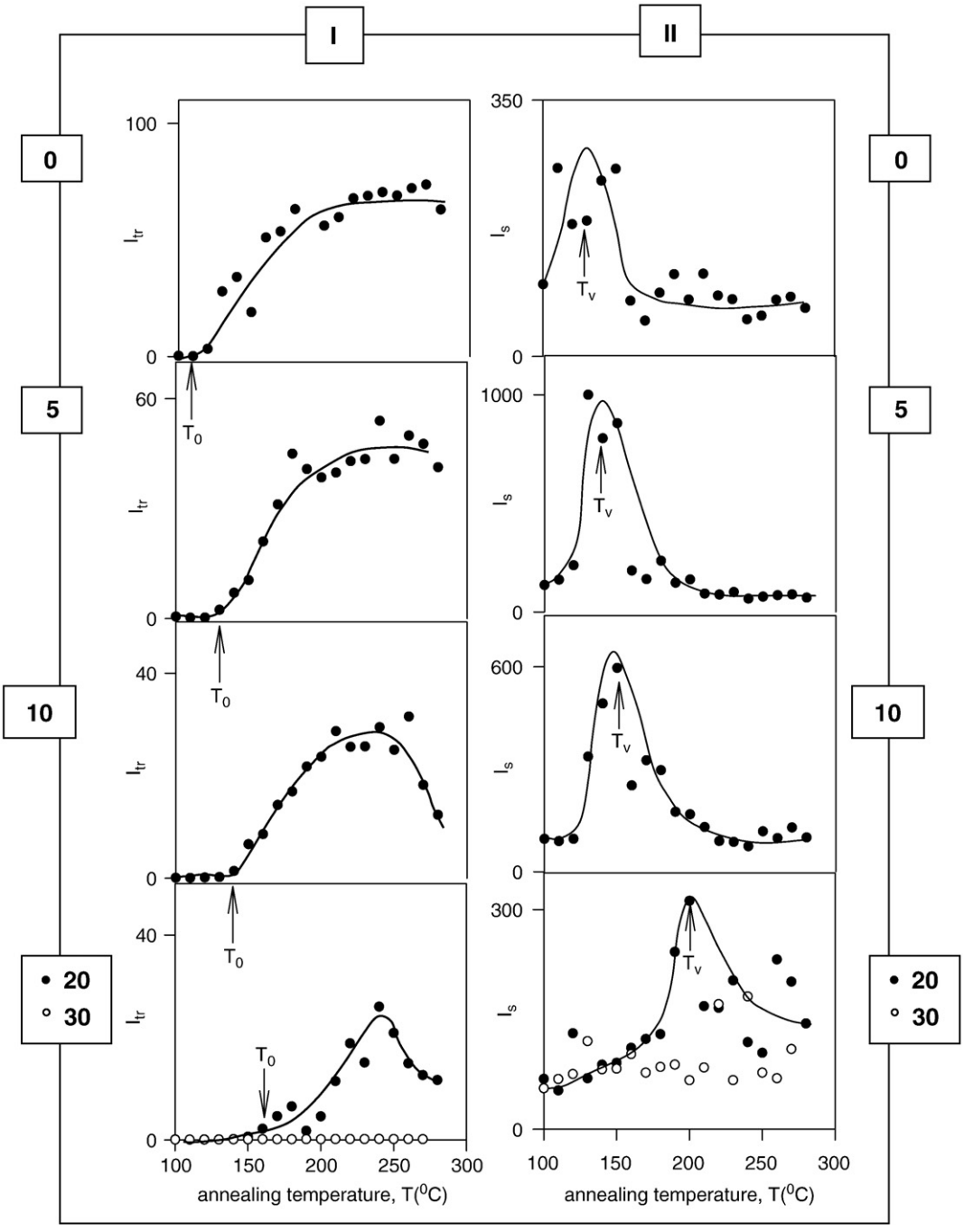


Fig. 4. Plot of (I) I_{tr} and (II) I_s intensities from composite films with different MLB content versus annealing temperatures. Numbers show MLB content in %.

3. Results and discussion

The emission (I_P) and scattered (I_s) spectra of the composite film with 10 wt.% MLB annealed for 10 min at various temperatures are shown in Fig. 3. Here, both I_P and I_s behave similarly upon annealing presenting maxima at certain temperatures. Increase in I_s started at lower temperatures than the increase in I_P. I_{tr}, I_s and I_P versus annealing temperatures are plotted in Figs. 4(I,II) and 5(I), respectively for the films with 0, 5, 10, 20 and 30 wt.% MNaLB content. Upon annealing the transmitted light intensity, I_{tr} (Fig. 4I) started to increase above a certain onset temperature, called the minimum film formation temperature, T_0 for all film samples. T_0 moves slightly to higher temperatures as the MLB content increased. The sample with 30 wt.% MLB showed almost no transmittance by indicating that light transmission is completely blocked by clay particles in the composite film. Scattered light intensity, I_s (Fig. 4II) showed a peak for 0, 5, 10 and 20 wt.% composites at the single temperature called void closure temperature, T_v. No variation for I_s was observed as the annealing temperature is increased for the film that contains 30 wt.% MLB. I_s is scattered from the surface of the composite film. But, I_{tr} passes through the film. On the other hand, fluorescence intensity reached a maximum increasing annealing temperature (Fig. 5I). The sample with 30 wt.% MLB showed almost no fluorescence emission. The photon diffusion in the composite films was blocked by the clay mineral particles. To eliminate the surface effect on the fluorescence intensity, the emission intensity at 395 nm was corrected by taking into account the scattered light from the surface of the film (Fig. 5II). The temperature where the I_P/I_s ratio reached the maximum is named the healing temperature, T_h.

The increase in I_{tr} above T_0 can be explained by the evolution of transparency of the composite films upon annealing. Most probably,

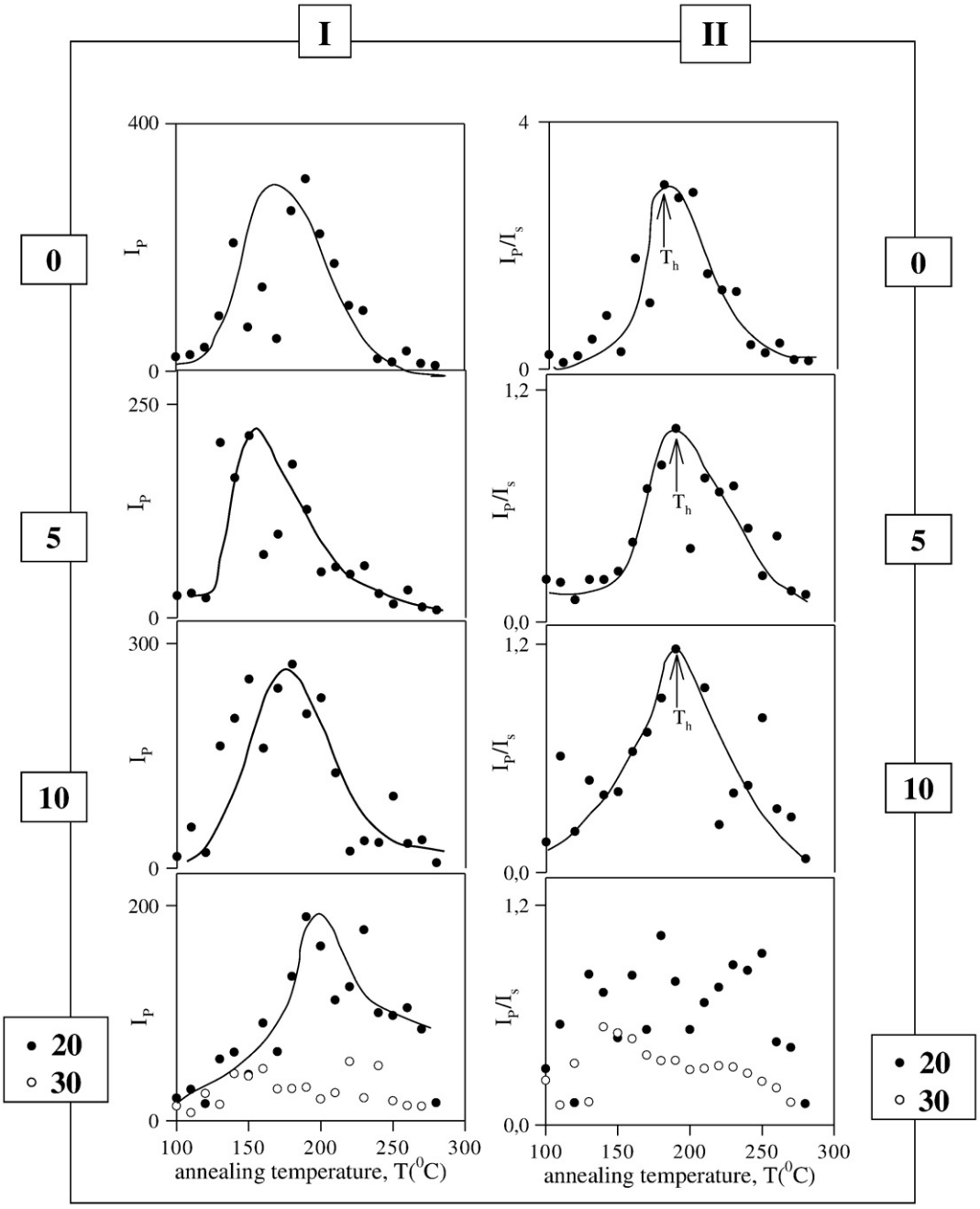


Fig. 5. Plot of (I) I_s and (II) corrected intensities (I_P/I_s) of composite films with different MLB content versus annealing temperatures. Numbers show MLB content in %.

the increase of I_{tr} corresponds to the void closure process, i.e. the polystyrene starts to flow upon annealing and voids between particles are filled. The sharp increase in I_s occurs at a certain temperature, below which light scatters isotropically because of the rough surface of the composite films. Annealing of the film at this temperature creates a flat surface which acts like a mirror and light is reflected to the photomultiplier detector. Further annealing makes the PS film transparent and I_s becomes minimum.

The increase of I_P above T_0 presumably corresponds to the void closure process up to the healing point. The decrease in I_P above T_h was understood as the interdiffusion process between polymer chains at the junction surface (Fig. 6).

It is well established that the variation in I_P depends on the mean optical path (total distance that the photon travels in the film) of a photon in the film (Canpolat and Pekcan, 1996; Ugur et al., 2003). This mean optical path is directly proportional to the probability of the photon encountering a pyrene molecule. If the optical path is large, the probability of the photon encountering a pyrene molecule is high. In Fig. 6a, before annealing, the mean free path (the distance where the photon takes in the film without scattering) is of the order of the size of the particle and interparticle voids. Since the film contains lot of voids, most of the light is scattered (I_s) at the air–polymer interface. After a few steps, the photon reemerges from the front surface of the film. Thus, the mean free and optical paths of a photon are very short yielding very low I_P. Fig. 6b shows a film in which interparticle voids disappeared due to annealing. After the void closure process completed, scattering takes place predominantly from the PS–PS and PS–MLB particle interfaces and the mean free path is of the order of the latex particle size. In this regime, (with the same number of rescatterings) a photon will stay for a much longer time in the film which gives rise to a long mean free and optical path in the film and I_P will increase. Finally, Fig. 6c presents the almost transparent film with no voids but some of MLB particles in the film. At this stage, the film has a low I_P because the mean free path and the optical path become of the order of the film thickness. This picture can be observed for the film with 30% MLB. For samples with higher MNaLB content, the fluorescence method cannot be applied to study film formation process. Because of the high opacity of the samples blocks the journey of the photon in the film and prevents fluorescence emission.

The plots of the maximum values of $(I_{tr})_{max}$ versus MLB content in Fig. 7 also confirms this picture. As the MLB content increased, $(I_{tr})_{max}$ showed a sudden decrease at 20 wt.% MLB, predicting a percolation threshold (p_c) behavior of MLB in the polymer matrix (Stauffer, 1985). At p_c, MLB percolates among the latex film, below p_c however transparency of the films is high and latex film formation was completed. In other words, despite the presence of MLB barriers

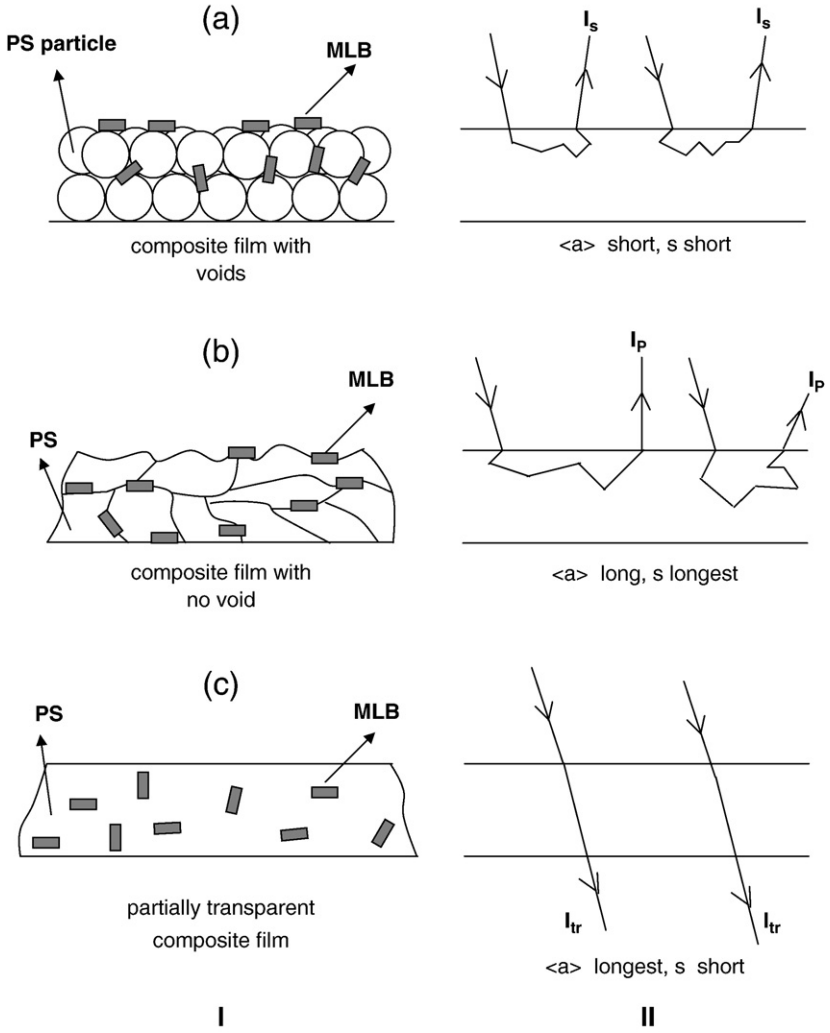


Fig. 6. Schematic illustration of the (I) composite film formation from clay mineral content latex particles and (II) variation in mean free and optical paths (<a> and s) during film formation; (a), (b) and (c) correspond to the film formation stages such as (a) film in powder form, (b) film after void closure process is completed, (c) partially transparent film.

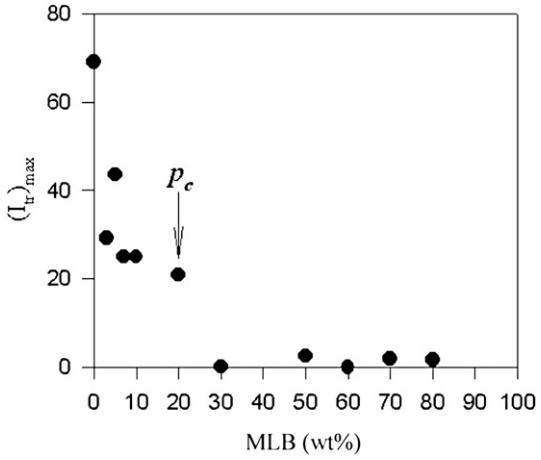


Fig. 7. Plot of the maxima of transmitted light intensities, $(I_{tr})_{max}$ from Fig. 4(I) versus MLB content.

polymer chains can interdiffuse across the particle–particle boundaries and a continuous film is formed. Above p_c, films become completely opaque. Since the size of MLB particles are large with respect to the wavelength of the visible light, most of the light is scattered which results in opacity in the film.

All results showed that the presence of MLB clay in the latex blocks and/or delays the film formation steps. To support these results, AFM micrographs of composite films were taken. Figs. 8 and 9 show the AFM pictures of 0, 7, 20 and 30% MLB content films annealed at 100 and 170 °C. No deformation in particles is observed for pure PS film (Fig. 8a). Films containing 7, 20 and 30 wt.% MLB (Fig. 8b, c and d) show a rough surface structures increasing the MLB content. After annealing at 170 °C (Fig. 9), AFM images clearly present the coalescence of PS particles for 0 and 7 wt.% MLB (Fig. 9a and b). The shape of the PS particles is destroyed and the microstructure of the latex has been disappeared completely. The film surface is relatively even and smooth predicting that interdiffusion processes completed and a mechanically strong continuous film is formed. However, some particle traces are seen on the surface for the films with 20 and 30 wt.% MLB (Fig. 11c and d), predicting that the existence of MLB protects some of the PS particles and therefore some PS particles were not destroyed during annealing. As a result, AFM data show that 20 wt.% MLB content presents a critical value, below which latex film formation in PS matrix takes place.

The increase in I_{tr} above T_0 for the (0–20) wt.% MLB range films can be explained with the void closure and/or surface smoothing processes by annealing. Similarly, the increase in I_P/I_s above T_0 presumably corresponds to the void closure process up to the T_h point where the healing process takes place. Decrease in I_P/I_s above T_h can be understood by interdiffusion between polymer chains.

3.1. Voids closure

In order to quantify the behavior of I_P/I_s and I_{tr} above T_0, a phenomenological void closure model is introduced. Latex deformation

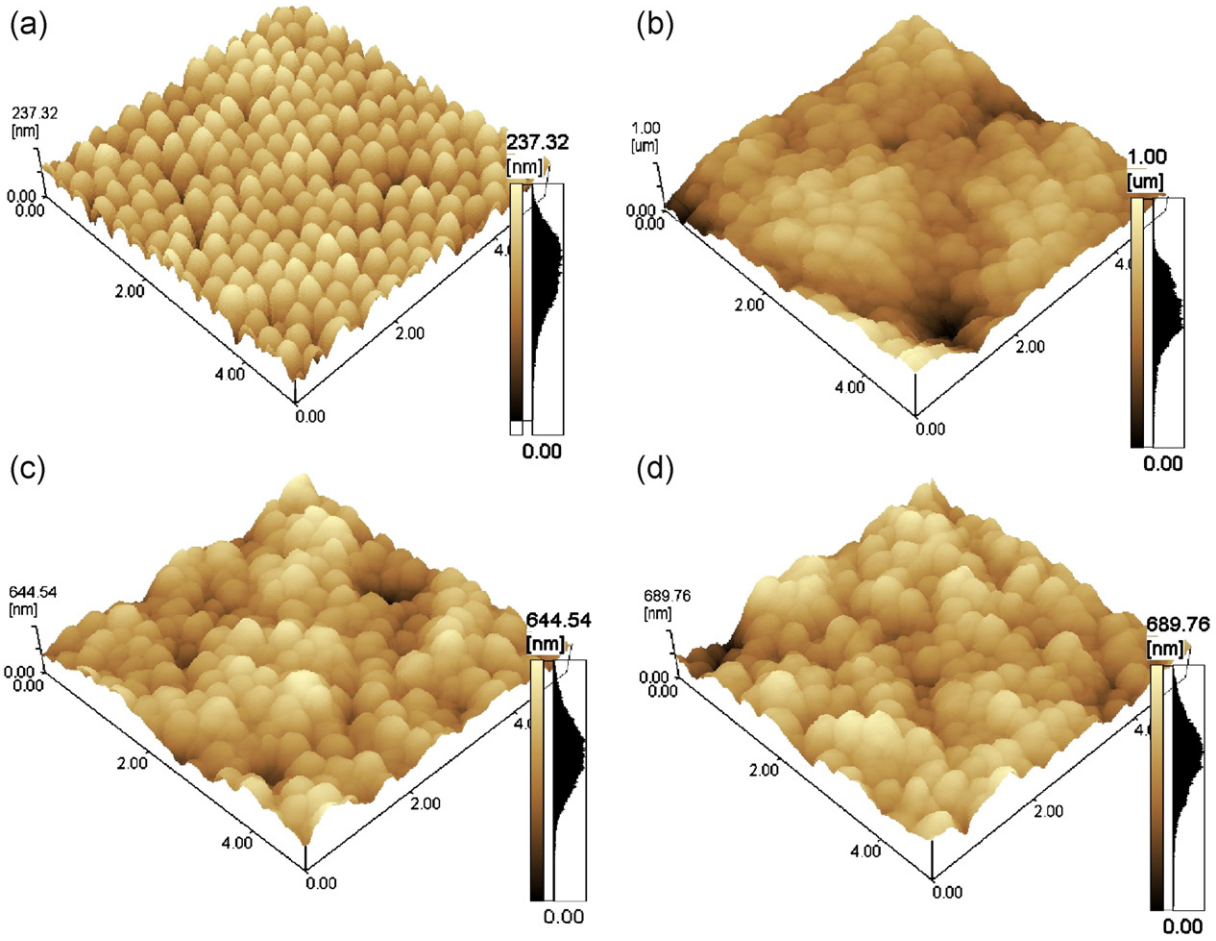


Fig. 8. AFM micrographs of composite films prepared with a — 0%, b — 7%, c — 20% and d — 30% MLB content and annealed at 100 °C for 10 min.

and void closure between particles can be induced by the shearing stress which is generated by surface tension of polymer i.e. polymer–air interfacial tension. The void closure kinetics adjusts the time for optical transparency and latex film formation (Keddie et al., 1996). To relate the shrinkage of spherical void of radius, r to the viscosity of surrounding medium, η an expression was derived and given by the following relation (Keddie et al., 1996).

$$\frac{dr}{dt} = -\frac{\gamma}{2\eta}\left(\frac{1}{\rho(r)}\right) \tag{1}$$

where γ is surface energy, t is time and $\rho(r)$ is the relative density. Here the surface energy causes a decrease in void size and the term $\rho(r)$ varies with the microstructural characteristics of the material, such as the number of voids, the initial particle size and packing. Eq. (1)) is similar to the one that was used to explain the time dependence of the minimum film formation temperature during latex film formation (Vogel, 1922; Mc Kenna, 1989). If the viscosity is constant in time, integration of Eq. (1) gives the relation as

$$t = -\frac{2\eta}{\gamma}\int_{r_o}^{r}\rho(r)dr \tag{2}$$

where r_o is the initial void radius at time $t=0$.

The dependence of the viscosity of the polymer melt on temperature is affected by overcoming the forces of macromolecular interaction which enables the segments of polymer chain to jump from one equilibration position to another. This process occurs at temperatures at which the free volume becomes large enough and is connected with the overcoming of the potential barrier. The Frenkel–Eyring theory produces the following relation for the temperature dependence of viscosity (Fulcher, 1925; Frenkel, 1945).

$$\eta = \frac{N_o h}{V}\exp\left(\Delta G/kT\right) \tag{3}$$

Where N_o is the Avogadro's number, h is the Planck's constant, V the is molar volume and k is the Boltzmann constant. By replacing $\Delta G=\Delta H-T\Delta S$ in Eq. (3)

$$\eta = A\exp\left(\Delta H/kT\right). \tag{4}$$

Where ΔH is the activation energy of viscous flow i.e. the amount of heat which 1 mol of material needs for creating the act of a jump during viscous flow. Here A represents a constant for parameters which do not depend on temperature. Combining Eqs. (2) and (4);

$$t = -\frac{2A}{\gamma}\exp\left(\frac{\Delta H}{kT}\right)\int_{r_o}^{r}\rho(r)dr. \tag{5}$$

To quantify the above results, Eq. (5) can be employed by assuming that the interparticle voids are equal in size and the number of voids is constant during film formation (i.e. $\rho(r)\propto r^{-3}$), then integration of Eq. (5) gives

$$t = \frac{2AC}{\gamma}\exp\left(\frac{\Delta H}{kT}\right)\left(\frac{1}{r^2}-\frac{1}{r_o^2}\right) \tag{6}$$

C is a constant related to relative density $\rho(r)$. As we stated before, a decrease in void size (r) causes an increase in mean free path <a> of a

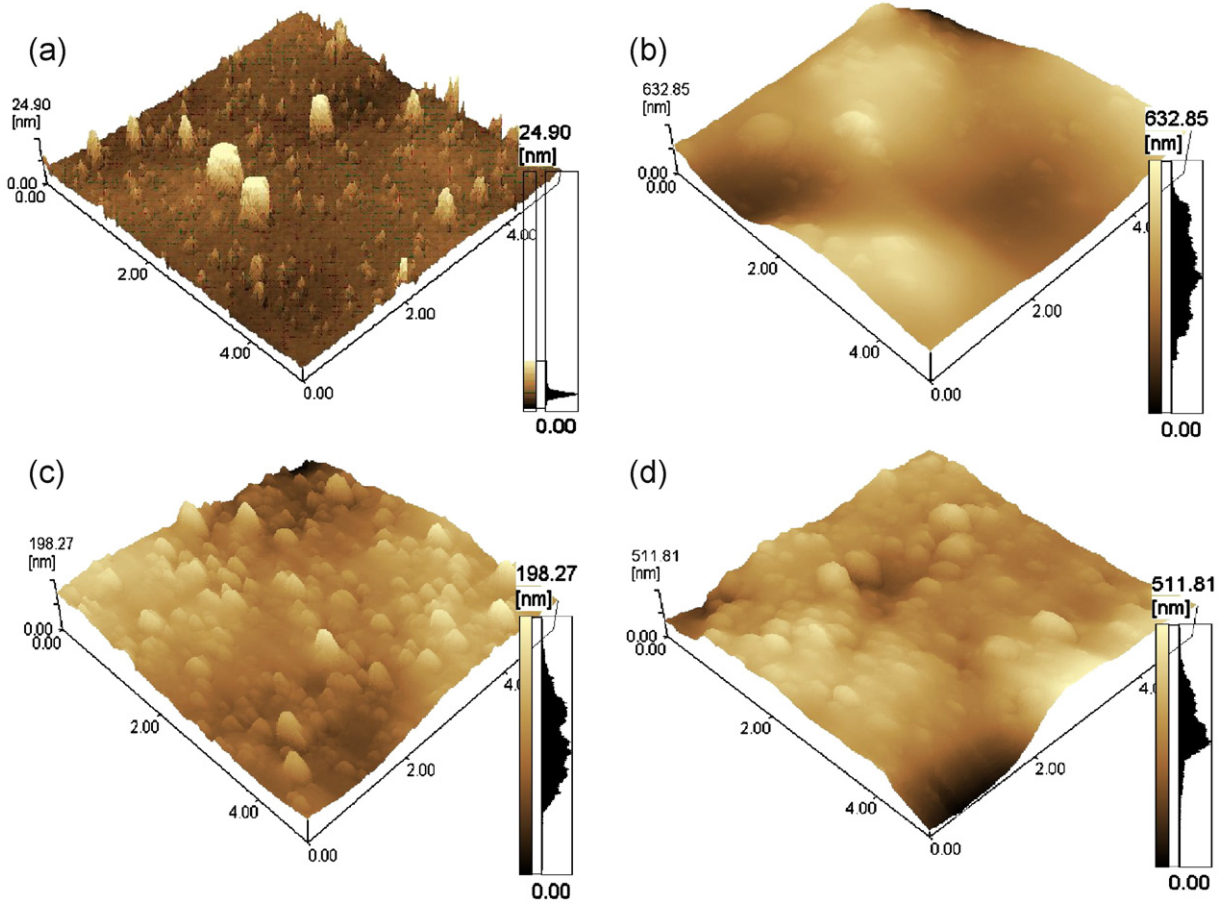


Fig. 9. AFM micrographs of composite films prepared with a — 0%, b — 7%, c — 20% and d — 30% MLB content annealed at 170 °C for 10 min.

photon, which then results an increase in I_{tr} and I_P intensities. This picture can also be visualized by Frenkel's neck formation model (Wu and Lerner, 1993), which takes into account identical contacting spheres under the influence of surface tension. Frenkel's model assumes that the displaced volume is redistributed uniformly such that the remaining surfaces keep their spherical shapes but of larger radii, which offers a larger mean free path <a> of a photon during its journey in the latex film. On the other hand, it is well known that scattering intensity increases with volume squared (the 6th power of radius) of scattering object (Voyutskii, 1963). If the assumption is made that emission and/or transmitted light intensity, I is inversely proportional to the 6th power of void radius, r then Eq. (6) can be written as

$$t = \frac{2AC}{\gamma} \exp\left(\frac{\Delta H}{kT}\right) I^{1/3}. \quad (7)$$

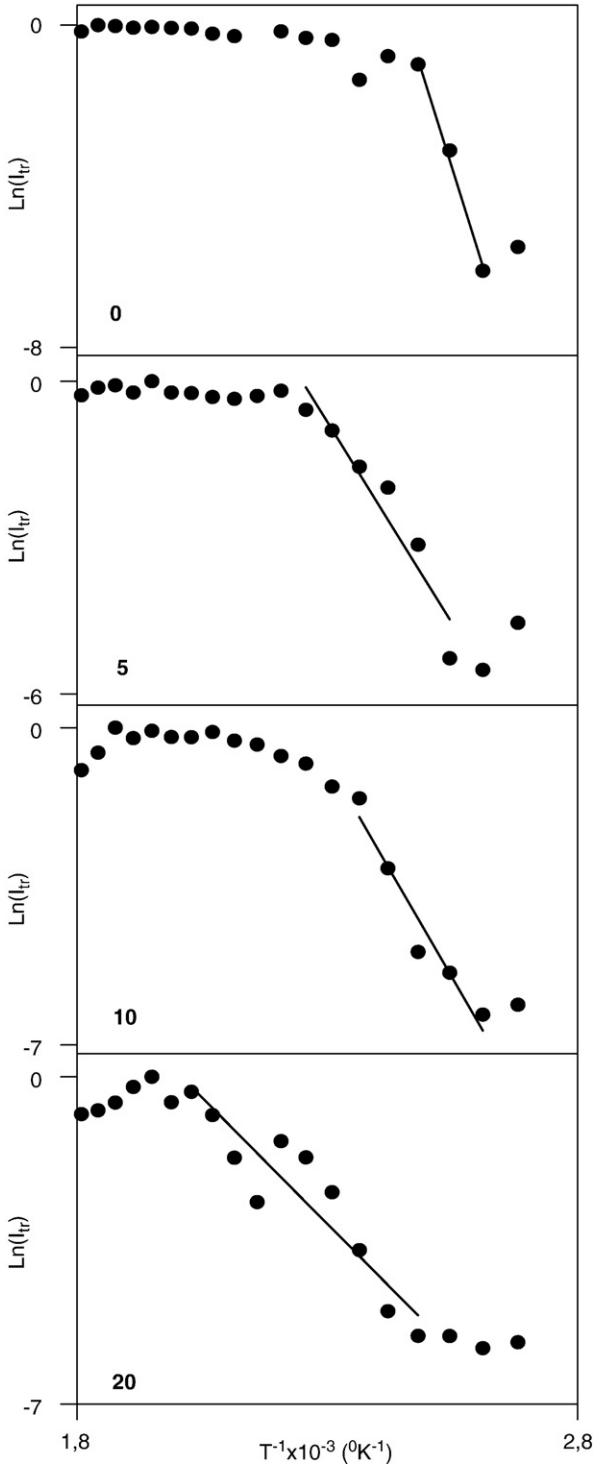


Fig. 10. Logarithmic plots of I_{tr} data versus inverse of annealing temperatures (T^{-1}) for the 0, 5, 10 and 20% MLB content films annealed for 10 min.

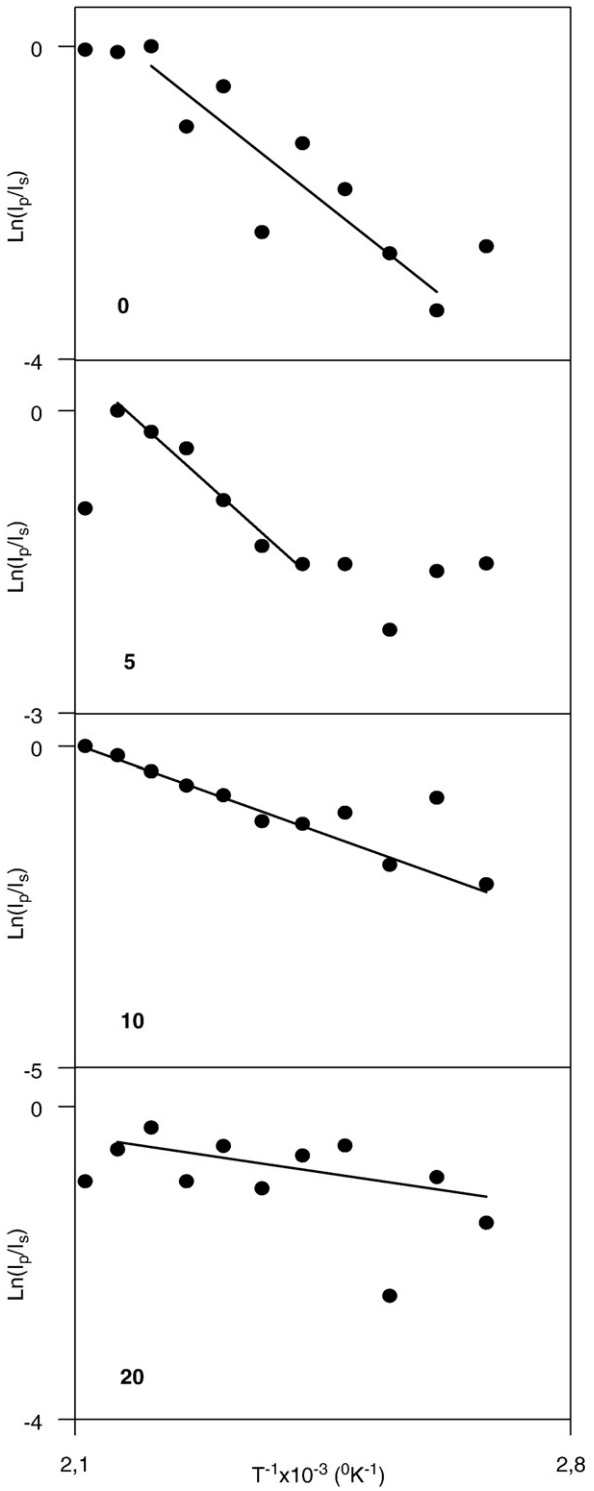


Fig. 11. Logarithmic plots of (I_P/I_s) data and fits to Eq. (9) below the healing point in Fig. 5 (II) for the 0, 5, 10 and 20% MLB content films annealed for 10 min.

Here, r_o^{-2} is omitted since it is very small compared to r^{-2} values after the void closure process. Eq. (7) can be solved for I to interpret the results in Figs. 4 and 7 as

$$I(T) = S(t)\ \exp\left(-\frac{3\Delta H}{kT}\right) \tag{8}$$

where $S(t)=(\gamma t/2AC)^3$. For a given time the logarithmic form of Eq. (8) can be written as follows

$$\mathrm{Ln}\, I(T) = \mathrm{Ln}\, S(t) - \left(\frac{3\Delta H}{kT}\right). \tag{9}$$

As it was already argued that the increase in I_{tr} and I_P/I_s originates from the void closure process, then Eq. (9) was applied to I_{tr} and I_P/I_s between the range of T_0 and T_h for all film samples except 30% MLB film. Figs. 10 and 11 present the LnI_{tr} and Ln(I_P/I_s) versus T^{-1} plots from the left hand side of the data in Figs. 4I and 5II, respectively from which ΔH_{tr} and ΔH_P activation energies were obtained. The measured void closure, ΔH_{tr} and ΔH_P activation energies are listed in Table 1. The results in Table 1 show that the activation energy decreases by increasing MLB content. The presence of the clay minerals in the latex system considerably lowers activation energies. In other words, the presence of MLB below 30 wt.% promotes the void closure process. As a result the latex film formation can be accomplished with much less energy. It has to be noted that the measured activation energies for viscous flow were found to be different in different techniques i. e. ΔH_P values are found much lower than ΔH_{tr} values. Since pyrenes are labeled to PS chain, it is believed that ΔH_P values are more realistic to interpret the viscous flow. On the other hand, ΔH_{tr} values were obtained indirectly compared to ΔH_P values.

3.2. Healing and interdiffusion

The decrease in I_P was already explained in the previous section, by the increase in transparency of latex film due to disappearing of deformed particle–particle interfaces. As the annealing temperature was increased above T_h, some part of the polymer chains may cross the junction surface and particle boundaries start to disappear, as a result I_P decreases due to the shorter optical path, s of a photon. To quantify these results, the Prager–Tirrell (PT) model (Prager and Tirrell, 1981; Wool et al., 1989) for the chain crossing density can be employed. These authors used de Gennes's "reptation" model to explain configurational relaxation at the polymer–polymer junction where each polymer chain is considered to be confined to a tube in which executes a random back and forth motion. A homopolymer chain with N freely jointed segments of length L was considered by PT, which moves back and forth by one segment with a frequency v. In time the chain displaces down the tube by a number of segments, m. Here, $v/2$ is called the "diffusion coefficient" of m in one dimensional motion. PT calculated the probability of the net displacement with m during time t in the range of $n-\Delta$ to $n-(\Delta+d\Delta)$ segments. A Gaussian probability density was obtained for small times and large N. The total "crossing density" $\sigma(t)$ (chains per unit area) at junction surface then was calculated from the contributions $\sigma_1(t)$ due to chains still retaining some portion of their initial tubes, plus a remainder, $\sigma_2(t)$.

Table 1
Probability of NaLB and MLB particles with size R

R (μm)	P_{NaLB} (%)	P_{MLB} (%)
50	0	–
40	13.5	–
30	22.8	–
20	33.3	–
10	49.8	–
8	51.2	4
6	51.2	12.5
5	53.6	15.6
4	56.4	17.9
3	59.1	22.3
2	63	32.7
1	69.9	56.2
0.8	72.2	63.6
0.6	75.4	71.1
0.5	–	75.2
0.4	–	79.8

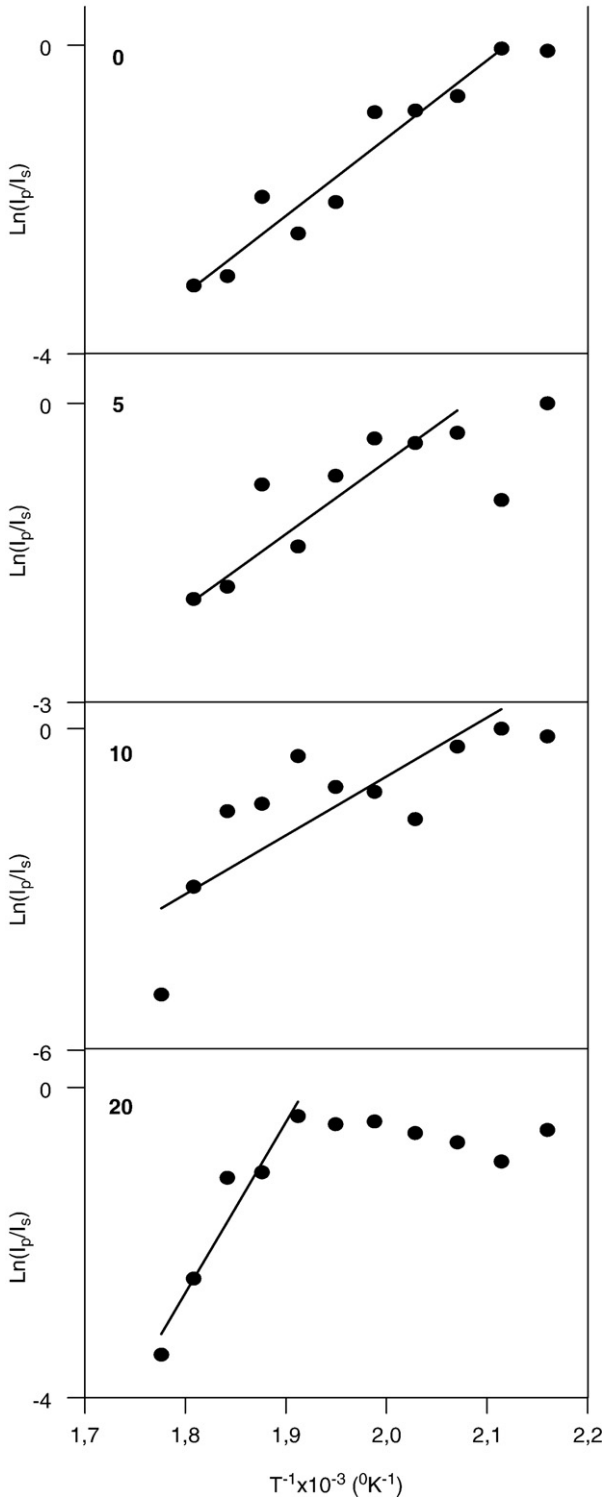


Fig. 12. Logarithmic plots of I_P/I_s and their fit to Eq. (15) above the healing point in Fig. 5 (II) for the films with 0, 5, 10 and 20 MLB contents.

Here the $\sigma_2(t)$ contribution comes from chains which have relaxed at least once. In terms of reduced time $\tau = 2vt/N^2$ the total crossing density can be written as

$$\sigma(\tau)/\sigma(\infty) = 2\pi^{-1/2}\left[\tau^{1/2} + 2\sum_{k=0}^{\infty}(-1)^n\left[\tau^{1/2}\exp\left(-k^2/\tau\right) - \pi^{-1/2}\,\mathrm{erfc}\left(k/\tau^{1/2}\right)\right]\right]. \quad (11)$$

For small τ values the summation term of the above equation is very small and can be neglected, which then results in

$$\sigma(\tau)/\sigma(\infty) = 2\pi^{-1/2}\tau^{1/2}. \quad (12)$$

This was predicted by de Gennes on the basis of scaling arguments (de Gennes, 1982). Here it should be mentioned that the dependence on time, t in Eq. (12) goes as $t^{1/4}$ at early times of healing (Wool and O'Connor, 1981; Kim and Wool, 1983). To compare our results with the crossing density of the PT model, the temperature dependence of $\sigma(\tau)/\sigma(\infty)$ can be modeled by taking into account the following Arrhenius relation for the linear diffusion coefficient

$$v = v_o \exp\left(-\Delta E_b/kT\right) \quad (13)$$

Here ΔE_b is defined as the activation energy for backbone motion depending on the temperature interval. Combining Eqs. (12) and (13) a useful relation is obtained as

$$\sigma(\tau)/\sigma(\infty) = R_o \exp\left(-\Delta E_b/2kT\right) \quad (14)$$

where $R_o = (8v_o t/\pi N^2)^{1/2}$ is a temperature independent coefficient.

The decrease in I_P/I_s in Fig. 5(II) above T_h is already related to the disappearance of particle–particle interfaces, i.e. as annealing temperature increased, more chains relaxed across the junction surface and as a result the crossing density increases. It can be assumed that I_P/I_s is inversely proportional to the crossing density $\sigma(T)$ then the phenomenological equation can be written as

$$I_P(T)/I_s(\infty) = R_o \exp\left(\Delta E_b/2kT\right). \quad (15)$$

Logarithmic plots of I_P/I_s versus T^{-1} are presented in Fig. 12 for samples with 0, 5, 10 and 20 wt.% MLB contents, respectively. The activation energy of backbone motion, ΔE_b is produced by least squares fitting the data in Fig. 12 to Eq. (15) and are listed in Table 2. ΔE_b values do not change with MLB content and are widely scattered. Below the percolation threshold, p_c of MLB (20 wt.%) interdiffusion can take place. Above p_c, polymer chains cannot interdiffuse across the boundary due to the screening effect of MLB, where the infinite network of MLB is constructed in the composite film. As a result, ΔE_b cannot be obtained for the composite sample of 30 wt.% MLB, most probably interdiffusion cannot be accomplished due to the percolation of MLB in the composite matrix. It is also seen that ΔE_b values are much higher than ΔH_P and ΔH_{tr}. Since the clay mineral particles can screen the motion of polymer chain across the junction, a single chain needs more energy to overcome this difficulty. Therefore a single chain needs more energy to diffuse across the polymer–polymer interface than bulk polymer needs.

Table 2
Experimentally produced activation energies

MLB content (wt.%)	ΔH_P (kcal/mol)	ΔH_{tr} (kcal/mol)	ΔE_b (kcal/mol)
0	4.74	26.22	40.05
3	3.93	12.2	39.57
5	4.18	10.26	28.91
7	3.57	10.37	10.06
10	2.6	12.63	43.66
20	0.89	7.14	87.56
30	–	–	–

ΔH_{tr}; activation energy of void closure (measured from I_{tr}).
ΔH_P; activation energy of void closure (measured from I_P).
ΔE_b; activation energy of backbone motion (measured from I_P).

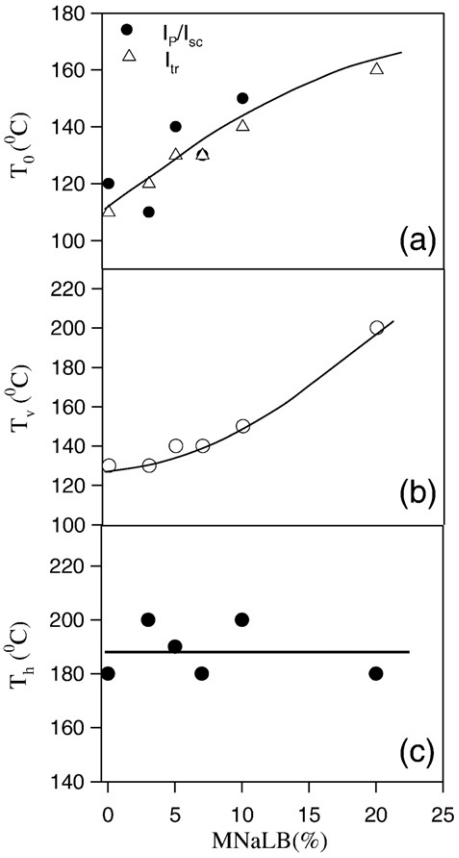


Fig. 13. The plots of a — minimum film formation, T_0, b — void closure, T_v and c — healing, T_h versus MLB content.

Finally, minimum film formation, T_0, void closure, T_v and healing, T_h, temperatures are plotted versus MLB content in Fig. 13a, b and c, where T_0 and T_v values increase with increasing MLB content (Fig. 13a and b). This behavior of T_0 and T_v clearly indicates that the existence of MLB delays the latex film formation process. However, healing processes are not affected by the presence of MLB (Fig. 13c), which is not surprising.

In conclusion, it was shown that film formation from PS latex and MLB particles can successfully be performed if the MLB content was below 20 wt.%. For (0–20) wt.% MLB all stages of film formation were observed. However, if the MLB content was above this critical value, 20 wt.% (percolation threshold) no film formation stages were observed. The morphological changes were found to be consistent with the SSF and UVV results.

References

Alexandre, M., Dubais, P., 2000. Polymer-layered silicate nanocomposites: preparation, properties and uses of a new class of materials. Mater. Sci. Eng. 28, 1–63.
Aranda, P., Ruizhitzky, E., 1992. poly(ethylene oxide)-silicate intercalation materials. Chem. Mater. 4, 1395–1403.
Canpolat, M., Pekcan, Ö., 1996. Healing and photon diffusion during sintering of high-T latex particles. J. Polym. Sci., Polym. Phys. Ed. 34, 691–698.
Collister, J., 2002. In: Vaia, R.A., Krishnamoorti, R. (Eds.), Polymer Nanocomposites; Synthesis, Characterization and Modeling. Oxford Univ. Press, London. Chap.2.
de Gennes, P.G., 1982. Kinetics of diffusion-controlled processes in dense polymer systems. II. Effects of entanglements. J. Chem. Phys. 76, 3322–3326.
Doh, J.G., Cho, I., 1998. Synthesis and properties of polystyrene organoammonium montmorillonite hybrid. Polym. Bull. 41, 511–518.
Frenkel, J., 1945. Viscous flow of crystalline bodies under the action of surface tension. J. Phys. (U.S.S.R) 9, 385–391.
Friedlander, H.Z., Grink, C.R., 1964. Organized polymerization III. Monomers intercalated in montmorillonite. J. Polym. Sci., Polym. Lett. 2, 475–479.

Fulcher, G.S., 1925. Analysis of recent measurements of the viscosity of glasses. J. Am. Ceram. Soc. 8, 339–355.
Giannelis, E.P., 1996. Polymer layered silicate nanocomposites. Adv. Mater. 8, 29–35.
Günister, E., Güngör, N., Ece, Ö.I., 2006. The investigations of influence of BDTDACl and DTABr surfactants on rheologic, electrokinetic and XRD properties of Na-activated bentonite dispersions. Mater. Lett. 60, 666–673.
Günister, E., Unlu, C.H., Atici, O., Ece, O.I., Gungor, N., 2007. Interactions of BDTDACl and DTABr surfactants with montmorillonite in aqueous systems. J. Compos. Mater. 41 (2), 153–164.
Kato, C., Kuroda, K., Takahara, H., 1981. Preparation and electrical-properties of quaternary ammonium montmorillonite–polystyrene complexes. Clay Clay Miner. 29 (4), 294–298.
Kawasumi, M., Hasegawa, N., Kato, M., Ususki, A., Okada, A., 1997. Preparation and mechanical properties of polypropylene–clay hybrids. Macromolecules 30, 6333–6338.
Keddie, J.L., Meredith, P., Jones, R.A.L., Donald, A.M., 1996. Film formation in waterborne coatings. In: Provder, T., Winnik, M.A., Urban, M.W. (Eds.), ACS Symp. Ser., 648, pp. 332–348.
Kim, Y.H., Wool, R.P., 1983. A theory of healing at a polymer polymer interface. Macromolecules 16, 1115–1120.
Le Baron, P.C., Wang, Z., Pinnavaia, T., 1999. Polymer-layered silicate nanocomposites: an overview. Appl. Clay Sci. 15, 11–29.
Li, Y., Zhao, B., Xie, S.B., Zhang, S., 2003. Synthesis and properties of poly(methyl methacrylate)/montmorillonite (PMMA/MMT) nanocomposites. Polym. Int. 52, 892–898.
Mackenzie, J.K., Shuttleworth, R., 1949. A phenomenological theory of sintering. Proc. Phys. Soc. B62 (No:12), 838–852.
Mazur, S., 1995. Coalescence of polymer particles. In: Rosenweig, N. (Ed.), Polymer Powder Processing. John Wiley and Sons.
McKenna, G.B., 1989. In: Booth, C., Price, C. (Eds.), Comprehensive Polymer Science, vol. 2. Pergamon Press, Oxford UK.
Noh, M.W., Lee, D.C., 1999. Synthesis and characterization of PS–clay nanocomposite by emulsion polymerization. Polym. Bull. 42, 619.
Pekcan, Ö., Arda, E., 1999. Void closure and interdiffusion in latex film formation by photon transmission and fluorescence methods. Colloids Surf., A Physicochem. Eng. Asp. 153, 537–549.
Prager, S., Tirrell, M., 1981. The healing-process at polymer–polymer interfaces. J. Chem. Phys. 75, 5194–5198.
Salahuddin, N., Akelah, A., 2002. Synthesis and characterization of poly (styrene–maleic anhydride)–montmorillonite nanocomposite. Polym. Adv. Technol. 13, 339.
Sperry, P.R., Synder, B.S., O'Dowd, M.L., Lesko, P.M., 1994. Role of water in particle deformation and compaction in latex film formation. Langmuir 10, 2619–2628.
Stauffer, D., 1985. Introduction to Percolation Theory. Taylor and Francis, London UK.
Ugur, S., Elaissari, A., Pekcan, Ö., 2003. Void closure and interdiffusion processes during latex film formation from surfactant-free polystyrene particles: a fluorescence study. J. Colloid Interface Sci. 263, 674–683.
Ugur, S., Alemdar, A., Pekcan, Ö., 2005. Films formed from polystyrene latex/clay composites: a fluorescence study. J. Coat. Technol. Res. 2 (7), 565–575.
Ugur, S., Alemdar, A., Pekcan, Ö., 2006. The effect of clay particles on film formation from polystyrene latex. Polym. Compos. 27, 299–308.
Usuki, A., Kojma, Y., Kawasumi, M., Okada, A., Fukuskima, Y., Kuvauchi, T., Kamigato, O., 1993. Synthesis of nylon 6-clay hybrid. J. Mater. Res. 8, 1179–1184.
Wang, Y., Zhang, Q., Fu, Q., 2003. Compatibilization of immiscible poly(propylene)/polystyrene blends using clay. Macromol. Rapid Commun. 24, 231–235.
Wool, R.P., O'Connor, K.M., 1981. A theory of crack healing in polymers. J. Appl. Phys. 52, 5953–5963.
Wool, R.P., Yuan, B.L., McGarel, O.J., 1989. Welding of polymer interfaces. J. Polym. Eng. Sci. 29, 1340–1367.
Wu, J., Lerner, M.M., 1993. Structural, thermal, and electrical characterization of layered nanocomposites derived from Na-montmorillonite and polyethers. Chem. Mater. 5, 835–838.
Vaia, R.A., Vasudevan, S., Krawiec, W., Scalon, L.G., Giannelis, E.P., 1995. New polymer electrolyte nanocomposites — melt intercalation of poly(ethylene oxide) in mica-type silicates. Adv. Mater. 7, 154–156.
Vara, R.A., Jandt, K.D., Kramer, F.J., Giannelis, F.P., 1996. Microstructural evolution of melt intercalated polymer-organically modified layered silicates nanocomposites. Chem. Mater. 8, 2628–2635.
Vogel, H., 1922. The law of relation between the viscosity of liquids and the temperature. Phys. Z. 22, 645–646.
Voyutskii, S., 1963. Colloid Chemistry. MIR Publisher, Moscow.